

Massively-Parallel Neuromonitoring and Neurostimulation Rodent Headset With Nanotextured Flexible Microelectrodes

Arezu Bagheri, *Student Member, IEEE*, S. R. I. Gabran, *Member, IEEE*, Muhammad Tariqus Salam, *Member, IEEE*, Jose Luis Perez Velazquez, Raafat R. Mansour, *Fellow, IEEE*, M. M. A. Salama, *Fellow, IEEE*, and Roman Genov, *Senior Member, IEEE*

Abstract—We present a compact wireless headset for simultaneous multi-site neuromonitoring and neurostimulation in the rodent brain. The system comprises flexible-shaft microelectrodes, neural amplifiers, neurostimulators, a digital time-division multiplexer (TDM), a micro-controller and a ZigBee wireless transmitter. The system is built by parallelizing up to four 0.35 μm CMOS integrated circuits (each having 256 neural amplifiers and 64 neurostimulators) to provide a total maximum of 1024 neural amplifiers and 256 neurostimulators. Each bipolar neural amplifier features 54 dB–72 dB adjustable gain, 1 Hz–5 kHz adjustable bandwidth with an input-referred noise of 7.99 μV_{rms} and dissipates 12.9 μW . Each current-mode bipolar neurostimulator generates programmable arbitrary-waveform biphasic current in the range of 20–250 μA and dissipates 2.6 μW in the stand-by mode. Reconfigurability is provided by stacking a set of dedicated mini-PCBs that share a common signaling bus within as small as $22 \times 30 \times 15 \text{ mm}^3$ volume. The system features flexible polyimide-based microelectrode array design that is not brittle and increases pad packing density. Pad nanotexturing by electrodeposition reduces the electrode-tissue interface impedance from an average of 2 M Ω to 30 k Ω at 100 Hz. The rodent headset and the microelectrode array have been experimentally validated *in vivo* in freely moving rats for two months. We demonstrate 92.8 percent seizure rate reduction by responsive neurostimulation in an acute epilepsy rat model.

Index Terms—Brain, extracellular recording, flexible microelectrode array, hippocampus, multichannel neural recording, multichannel neural stimulation, rodent headset.

I. INTRODUCTION

SIMULTANEOUS monitoring of electrical neural activity at many locations in the brain provides electrographic data with high spatial resolution. This enables investigation

Manuscript received March 22, 2013; revised June 14, 2013; accepted July 07, 2013. Date of publication October 17, 2013; date of current version October 24, 2013. This work was supported by the Natural Sciences and Engineering Research Council of Canada, the Ontario Brain Institute, and the Canadian Microelectronics Corporation (CMC). The authors also thank these organizations for their technical support and Y. Adamchik for animal care and handling. This paper was recommended by Associate Editor T.-P. Jung.

A. Bagheri, M. T. Salam, and R. Genov are with the Department of Electrical and Computer Engineering, University of Toronto, Toronto, ON M5S 3G4, Canada (e-mail: arezu@eecg.utoronto.ca).

S. R. I. Gabran, R. R. Mansour, and M. M. A. Salama are with the Department of Electrical and Computer Engineering, University of Waterloo, Waterloo, ON N2L 3G1, Canada.

J. L. Perez Velazquez is with the Brain and Behaviour Centre, Division of Neurology, University of Toronto, Toronto, ON M5G 1X8, Canada.

Color versions of one or more of the figures in this paper are available online at <http://ieeexplore.ieee.org>.

Digital Object Identifier 10.1109/TBCAS.2013.2281772

of the behavior of a large population of neurons and comprehensive neural activity assessment required for developing state-of-the-art neural prostheses, such as for treatment of medically refractory epilepsy [1]. Simultaneous electrical current stimulation localized at many sites in the brain allows for fine-tuned neurostimulation therapies optimized for a given neural disorder and custom-tailored to each specific patient, potentially increasing their efficacy. Combining both neural monitoring and neural stimulation in a single implantable device enables responsive neural stimulation, where stimulation is triggered by detected neural events, a promising paradigm in modern neuro-rehabilitation.

A steady increase in the number of monitored sites in the brain has been observed, approximately doubling every seven years [2]. Expanding the number of recording and stimulation sites introduces several challenges including noise, power consumption and form factor of electronic neural interfacing circuits as well as impedance and fragility of microelectrodes.

Multichannel commercial neural recording and stimulation systems for humans do not interface with many recording or stimulation sites (e.g., currently up to eight for responsive neurostimulation for treatment of medically refractory epilepsy). Animal models of neurological disorders, particularly rodent models, are widely accepted as low-cost vehicles for developing state-of-the-art neural prostheses. Commercial neural recording and stimulation products for implantation in rodents currently offer up to 32 channels [3]. In academia, Neurochip-2 at University of Washington has been very successful but weighs 145 g and has only three recording and three stimulation channels [4]. HermesD at Stanford University has 32 recording channels but no neurostimulation channels [5]. A number of other state-of-the-art headset designs have been reported [6], [7], but either have a limited number of channels, or lack neurostimulation, or have a large form factor.

Several microelectrode designs, mostly silicon-based, have been developed for multi-site neural recording and stimulation [8]–[10]. Silicon electrodes can cause post-operative trauma and damage to brain tissue due to their rigid structure. Silicon electrodes are brittle and would release debris in the brain upon mechanical failure and fracture. Additionally, the high packing density requirement necessitates reducing contact size, which increases its impedance, thus degrades the recording signal-to-noise ratio and the maximum stimulation current for a given supply voltage.

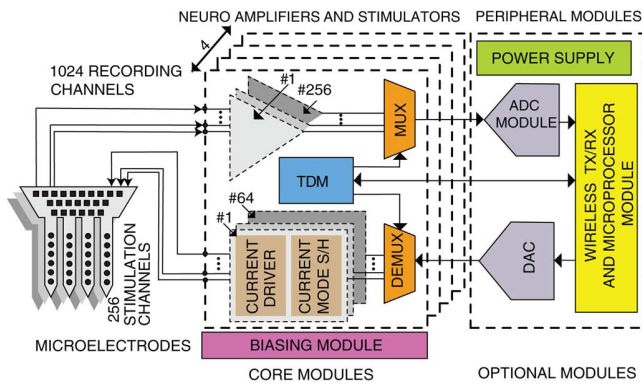


Fig. 1. System-level block diagram.

Massively-parallel integrated neural interfaces have a potential to improve our understanding of neurological disorders such as intractable epilepsy, and meliorate therapy development. Intractable epilepsy (also known as uncontrolled or refractory) is a seizure disorder in which patient seizures cannot be controlled with medication. Several therapeutic devices for treating intractable epilepsy have been introduced to replace conventional therapies which have low efficacy. Currently, vagus nerve stimulator (VNS) is the only medical device approved by FDA (Food and Drug Administration) for the treatment of intractable epilepsy patients in the US [11], [12]. However, the efficacy of this arbitrary (open-loop) stimulation device is limited to 3 percent for seizure freedom (i.e., observing no seizures for a period of 12 months) [13] and 30–40 percent for responder rate (i.e., showing more than 50 percent reduction in seizure frequency) [11], [12], [14]. Recently, Neuropace Inc. (Mountain View, CA) introduced the RNS (responsive neurostimulator) system that triggers electrical stimulation upon electrographic seizure onset detection [15]. This cranially implanted neurostimulator is designed to detect seizure activity in the brain and to deliver pre-defined electrical stimulation to suppress seizures. Preliminary results of this electrical stimulation therapy are acceptable, however, many patients do not respond well to this treatment, and this is hypothesized to be in part due to low recording and stimulation electrode count [16], [17].

In this paper, we present a compact wireless rodent headset with a maximum channel count of 1024 for simultaneous neural recording, and 256 for simultaneous neural stimulation. It is interfaced with flexible-shaft microelectrode arrays with tissue contact surface modified by nanotexturing to reduce its impedance on average by a factor of over 60. The system targets simultaneous large-scale neural monitoring, spatially-rich neural stimulation and closed-loop neurostimulation for studies of intractable epilepsy treatment in rodent seizure models. The block diagram of the system is shown in Fig. 1.

II. METHODS AND MATERIALS

The head-mounted system is comprised of two components: an electronic headset and a flexible microelectrode array.

A. Rodent Headset

The rodent headset consists of 2 core and 3 optional modules in the form of stacked miniature printed circuit boards (PCBs)

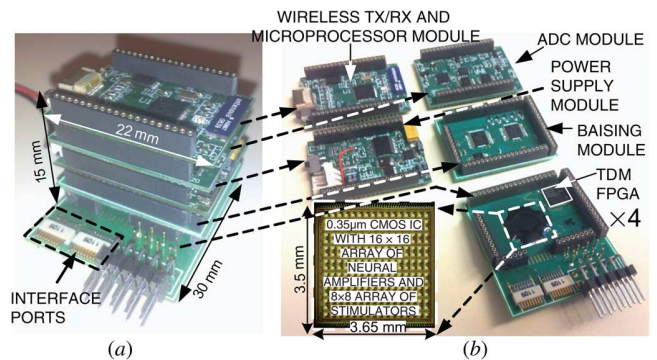


Fig. 2. Wireless headset. (a) Assembled stack. (b) Individual boards.

as shown in Fig. 2. Each module provides circuits for a distinct function, as described next. Using some of the modules is optional as the system is functional without them in a wired configuration with back-end bench-top equipment.

1) *Neural Amplifiers and Stimulators (Core1) Module*: A neuro-interface integrated circuit (chip) was designed and introduced in [18] to provide 256 recording and 64 stimulation channels. The chip is wire-bonded onto a 22 mm × 30 mm PCB module and is protected by epoxy. Four of these modules can be stacked to provide 1024 simultaneous recording channels and 256 stimulation channels. In this prototype only 64 channels were wirebonded for experimental testing. This module also features a small low-power FPGA to provide clocks and control signals to the chip and perform data processing.

The amplifier in each recording channel has a programmable mid-band gain from 54 dB to 72 dB, programmable bandwidth of 1 Hz to 5 kHz with $7.99 \mu\text{V}_{\text{rms}}$ input-referred noise. Each recording channel consumes $12.9 \mu\text{W}$ and occupies 0.02 mm^2 [18]. Microelectrodes are connected to the amplifier in a bipolar fashion through four Omnetics connector ports. The low-power FPGA performs time-domain multiplexing of these channels.

The bipolar stimulators feature charge-balanced symmetric biphasic stimulation which provides control over the charge delivered to the tissue. The delivered charge per phase is limited according to safe electrical stimulation model [19]. The stimulation current ranges from $20 \mu\text{A}$ to $250 \mu\text{A}$ and each stimulator consumes $2.6 \mu\text{W}$ quiescent power and occupies 0.03 mm^2 . Each stimulation channel can be individually addressed and the stimulation parameters are set by the on-board FPGA. A group of selected stimulation channels provide simultaneous stimulation without multiplexing.

2) *Biasing (Core2) Module*: The bias voltages and currents required by the neural recording and stimulation chip are generated by a set of DACs.

3) *Power Supply (Optional) Module*: The power supply module provides multiple regulated source voltages for different circuits of the system. Power is provided to this module from a small battery. The power supply board has programmable power-down mode for efficient power use and longer battery life. The system remains in the power down mode until certain amount of data is stored in the microcontroller for wireless transmission.

4) *ADC (Optional) Module*: The analog recorded data is fed to the ADC module to digitize the data.

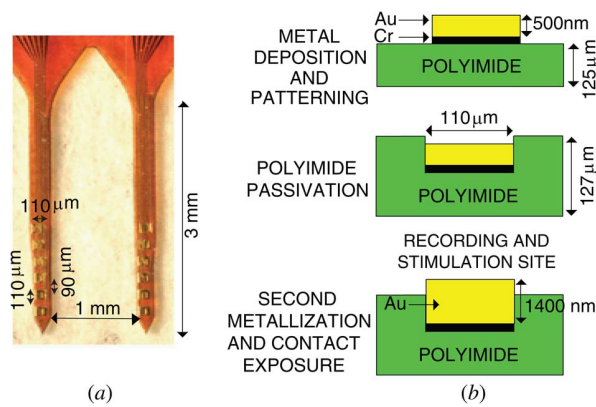


Fig. 3. Flexible microelectrode array example. (a) Photograph and dimensions. (b) Fabrication process (not to scale).

5) *Wireless Tx/Rx and Microprocessor (Optional) Module:* The digital data packets received from the ADC module can be transmitted through a ZigBee wireless connection. Commands can also be received wireless through the same interface. A TI microcontroller can be used in a closed-loop configuration. The wireless interface is included to facilitate debugging the neurostimulator in the closed-loop configuration.

This system is powered by a Lithium-sulfur dioxide battery (not shown), weighs 12 g (with the battery), and can operate for 10 hours continuously. The optional modules described in items 3 to 5 above were designed and fabricated by Canadian Microelectronics Corporation (CMC), in a joint research project.

B. Flexible Microelectrode Array

The microelectrodes provide a 2-D array of neural interfacing sites capable of both recording and stimulation through large-area pads. The electrode architecture was developed to maximize channel packing for a given set of electrode dimensions without increasing the shaft width.

1) *Electrode Mechanical Design:* During insertion and operation, the electrode is subjected to axial and shear loading and is susceptible to mechanical failure. Buckling failure is caused by axial loading if the insertion force exceeds the critical load of the electrode structure and will prevent tissue penetration. Moreover, the electrode is loaded with stresses during operation generated by vascular pulsatility, and these can cause fracture in the case of a brittle electrode structure. In order to address these issues, the microelectrode array is implemented on a flexible polyimide substrate. A finite element model was created to analyze the electrode mechanical performance. The microelectrode dimensions and geometry are designed to provide the required mechanical stability during tissue penetration to avoid buckling failure. The flexible structure allows the microelectrode to conform to the surrounding tissue and flex in response to the exerted shear forces without failure. The microelectrode is designed with tapered tips and its small footprint reduces tissue trauma and improves biocompatibility.

2) *Electrode Layout:* The developed architecture was employed to create a multi-shaft microelectrode array. Each shaft is 3 mm long and has a width of 130 μm . It accommodates six 110 μm \times 110 μm pads with pad spacing of 90 μm , as depicted in Fig. 3(a). The design is scalable and can provide more

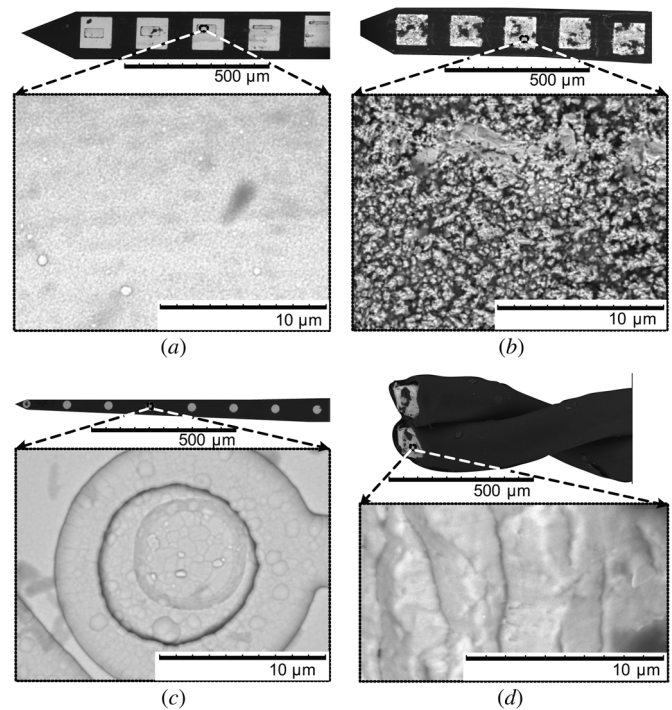


Fig. 4. Scanning electron microscope (SEM) images. (a) Smooth-surface microelectrode (SME). (b) Nanotextured microelectrode (NME). (c) Commercial microelectrode (CME). (d) Commercial microwire (CMW).

interface channels by increasing the number of shafts and layering multiple substrates onto each other. This has been experimentally validated. Each channel has an interconnect pad to couple the electrode to circuits using FFC/FPC connectors and cables (Molex 501616-2575). A custom printed circuit board is designed to provide standard pin header connection to the electrode channels to facilitate mating to other circuits.

3) *Fabrication Process:* Polyimide is a biocompatible polymer and was chosen as the structural layer due to its mechanical properties. The electrode is implemented on polyimide film, as shown in Fig. 3(b). The film, which is 125 μm thick, is cleaned in acetone and isopropanol alcohol baths, and then dehydrated on a hotplate. The metallization layers are made of gold. Chrome is used to improve adhesion between gold and polyimide, as shown in Fig. 3(b). Metal films are deposited using e-beam evaporation and DC sputtering for chrome (30 nm) and gold (500 nm) respectively. Metallization layers are patterned using photolithography and wet etching. Then polyimide passivation layer is spin coated and cured in a furnace according to the standard polyimide process recipe. Via holes are created in the passivation layer using aluminum mask and plasma etching, then the top metallization layer is deposited and patterned to create the exposed pads with a raised profile. Finally, the aluminum mask is wet etched and the electrode is diced and released using laser micromachining [20]. The fabrication process is illustrated in Fig. 3(b).

4) *Electrode Pad Surface Modification:* The surface impedance of the resulting microelectrode pads shown in Fig. 4(a) is approximately 2 M Ω at 100 Hz. In order to reduce the pad impedance, a pad surface modification technique was developed using low-current pulsed electroplating process to increase the pad surface roughness. Electroplating is performed

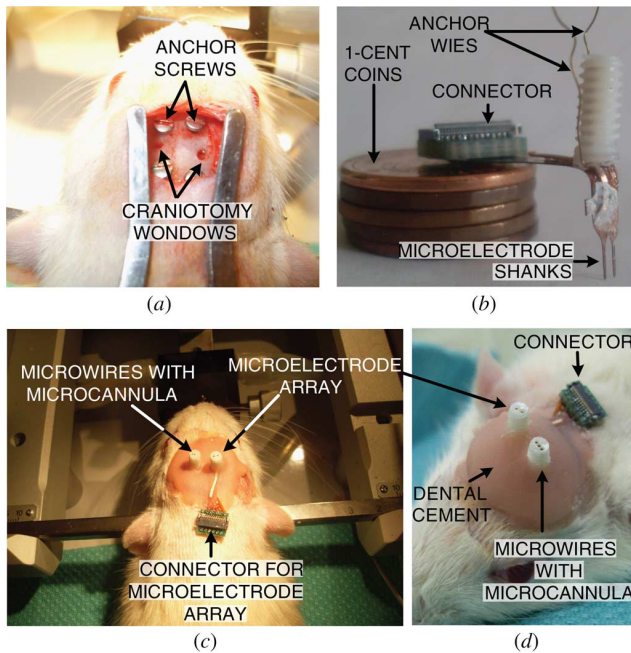


Fig. 5. Microelectrode implantation procedure in the rat brain. (a) Craniotomy windows created in the skull. (b) Customized flexible microelectrode array with its connector. (c) Microelectrode array and microcannula after the implantation. (d) Surgical site covered with dental cement.

using pure gold plating process (Technic Mini Plating Plant 3), in which a 30 mA current was applied in bursts of 20 seconds for 2 minutes. The resulting nanotextured electrodes (NME) exhibit rough surface, shown in Fig. 4(b), and an improved average impedance of approximately 30 k Ω at 100 Hz. Section III compares the performance of these microelectrodes with a commercial microelectrode (CME) and a commercial microwire (CMW) shown in Fig. 4(c) and (d), respectively.

C. Seizure Suppression by Closed-Loop Stimulation

Closed-loop stimulation studies were conducted at the Neuroscience & Mental Health Research Institute at the Hospital for Sick Children (Toronto, Canada) with an approval from its ethics committee.

1) *Microelectrode Array Implantation Procedure*: Six male Dawley rats (weight: 150–500 g) underwent craniotomy with general anaesthesia (using isoflurane and oxygen) as shown in Fig. 5(a). The animal hair was shaved and skin was pre-treated with atropine, lactate ringer USP and lidocaine. A small slit was created in the skin overlying the head to expose the skull. Four holes were drilled on the skull to place four anchor screws (with diameter of 1.25 mm) on top of the cerebellum, as shown in Fig. 5(a).

Craniotomy windows were drilled out on both sides. The flexible microelectrode array, shown in Fig. 5(b), was implanted in the somatosensory area in the right hippocampus, using a stereotaxic micro manipulator apparatus with steady forceps arms (Stoelting Co., Germany). On the other side, in the left hippocampus, a microwire with a microcannula (Plastics-1 Inc., Roanoke, VA, USA) was implanted similarly. Finally, the entire surgical site surface, skull, anchor screws, microelectrodes and microwires were covered and sealed with dental cement. The tip of the microcannular drug injection site,

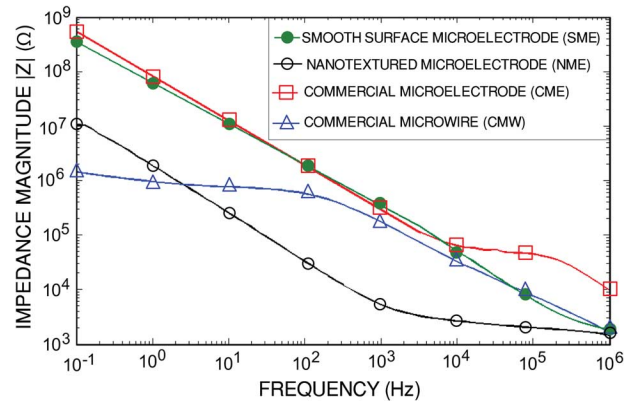


Fig. 6. Measured impedance of the presented and commercial electrodes.

the recording connector and the reference were left exposed as shown in Fig. 5(c) and (d).

After the implantation, each animal was under post-operative care for three consecutive days. After a 10-day post-operative recovery period, the freely-moving animals were placed in cages to perform intracranial EEG recording, monitored by video cameras. Intracranial EEG signals were monitored using the presented headset and the animal behaviors were recorded simultaneously by two video cameras.

2) *Chronic Basal Activity Recording*: Basal EEG signals and animal behaviors were monitored for 4 hours each day, 2 hours in daytime (12–2 p.m.) and 2 hours at night (12–2 a.m.) for a period of one week.

3) *Epileptic Seizure Induction Method*: Focal seizures were induced by intracerebral injection of 4-aminopyridine (4-AP). 300 nmol of 4-AP was diluted in 2 μ L of sterile 0.9 percent saline and was sonicated for two minutes to have uniform suspension and adequate concentration of the drug. Each rat was anesthetized with isoflurane and 8 μ L of 4-AP solution was injected through the microcannula into its hippocampus. After the injection, each rat was connected to the system for recording spontaneous recurrent electrographic seizures and was monitored by video cameras for clinically associated behaviors for 4 hours. The seizure behaviors were carefully monitored and noted according to the Racine scale [21].

4) *Seizure Onset Detection*: The epileptic seizure detection method was previously introduced by the authors in [22], [23]. It has been demonstrated that the phase locking value (PLV) between two or more EEG signals is a good precursor of ictal events and thus can be used to detect a seizure onset [24], [25]. PLV is proportional to the fluctuations in the phase difference of two channels and is calculated as $PLV = |d(\Delta\theta)/dt|$, where $\Delta\theta$ is the phase difference between the two selected channels. This seizure onset detection method was converted to a script in Matlab and used in a remote computer. It can also be implemented on the FPGA in the first core PCB module (Section II-A-1) for in-situ seizure onset detection.

5) *Closed-Loop Stimulation Method*: All seizure-induced animals were divided into two groups: (1) non-treatment group and (2) treatment group. In the non-treatment group (three rats), seizures were monitored, labeled and the seizure frequency per hour was determined. In the treatment group (three rats), the implanted microelectrode array was connected externally to the

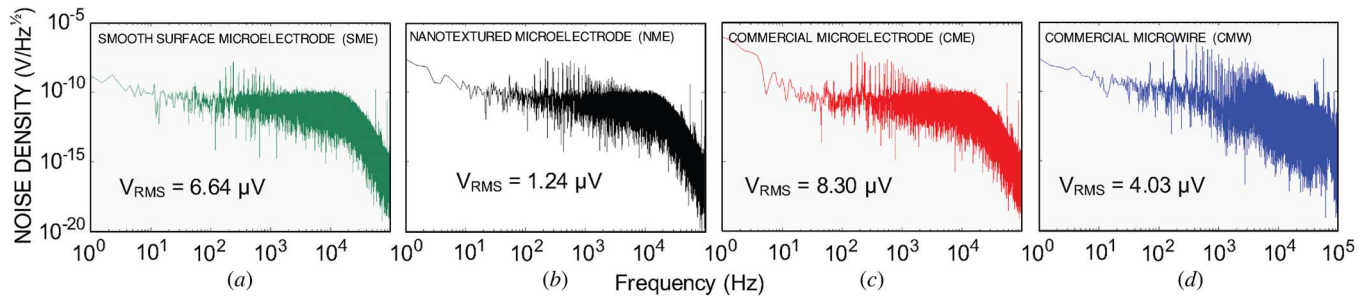


Fig. 7. Measured electrode noise spectral densities of the presented and commercial electrodes.

headset and the recorded EEG signals were sent to a computer to be analyzed by the seizure onset detection algorithm in Matlab every two seconds. The detector triggers the neurostimulators in the headset to send a burst of electrical stimulation current in response to a seizure onset detection.

III. EXPERIMENTAL RESULTS

The system has been used in comparing the performance of several electrodes including smooth-surface microelectrodes (SME), nanotextured microelectrodes (NME), commercial thin film microelectrodes (CME) and commercial microwires (CMW). Fig. 4(a)–(d) present the scanning electron microscope (SEM) images of these electrodes, respectively. The close-up views in Fig. 4 illustrate the surface condition of the metal pads. The NME exhibits the most roughened surface with the desired nano-scale structures clearly seen and yields the lowest impedance, as detailed next.

A. Microelectrodes Characterization

The electrode-tissue interface impedance of the presented and the commercial electrodes were measured using standard two-electrode electrochemical cell with 0.9 percent saline solution. The impedance magnitude versus frequency plots for the electrodes, obtained by impedance spectroscopy (Solatron SI 1260 Impedance/Gain-Phase Analyzer), are shown in Fig. 6. The presented rough surface nanotextured microelectrode (NME) exhibits significantly lower impedance in the 10 Hz to 100 kHz frequency band due to the increased effective surface area.

Electrode-electrolyte noise was measured using a large (2 cm \times 2 cm) platinum reference plate in a standard physiological saline solution. Fig. 7 illustrates electrode-electrolyte noise densities of the presented and commercial electrodes. The NME has the lowest noise density due to its lower impedance.

B. In Vivo Neural Signal Recording Performance

The recording performance of the four electrode types was evaluated in acute EEG signal recording using the rodent headset. The headset was also tested chronically *in vivo* in freely moving rats.

1) *Acute Recording*: One Dawley rat underwent a craniotomy with general anaesthesia. Through the craniotomy windows, four types of microelectrodes (Fig. 4) were implanted in the somatosensory area. Bipolar intracranial EEG recording was performed using the headset. The recorded signals have been analyzed in several frequency bands (delta 0.1–4 Hz, theta 4–7 Hz, alpha 8–13 Hz, beta 13–30 Hz, and

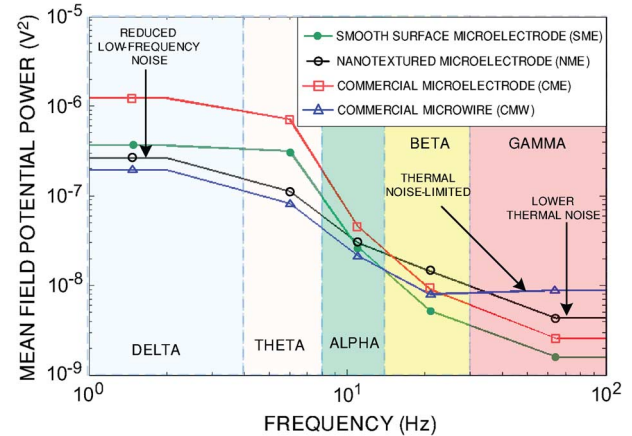


Fig. 8. Field potential power recorded from somatosensory area using the presented and commercial electrodes.

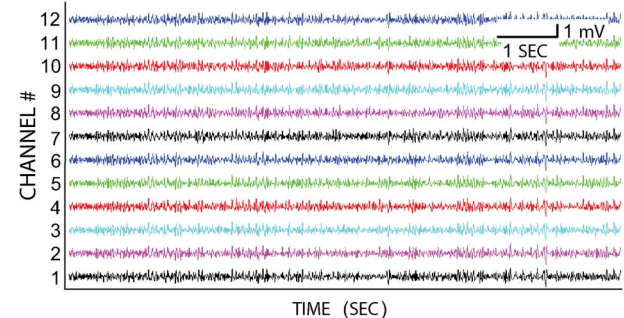


Fig. 9. Intracranial EEG signal from rat hippocampus recorded *in vivo* from 12 channels using the presented flexible microelectrode array and headset.

gamma 30–100 Hz). The mean field potential power in each band was measured in order to evaluate the recording quality, as shown in Fig. 8. Fig. 8 illustrates that CME and SME exhibit higher low-frequency noise whereas the low-frequency noise is suppressed when using NME and CMW. Fig. 8 also demonstrates that at high frequencies, NME exhibits lower thermal noise than that of CMW. Thus NME yields the best overall signal fidelity.

2) *Chronic Recording*: A dual-shaft flexible microelectrode array with 12 channels was implanted in the right hippocampus of a rat, as described in Section II-C-1. Two weeks after the implantation, field potentials were sampled at 1 kHz and band-pass filtered from 0.5 Hz to 500 Hz. Fig. 9 illustrates intracranial EEG recordings (3 weeks after the implantation) using the presented headset. The long-term recordings are stable without a significant decrement in signal quality for up to 9 weeks after implantation.

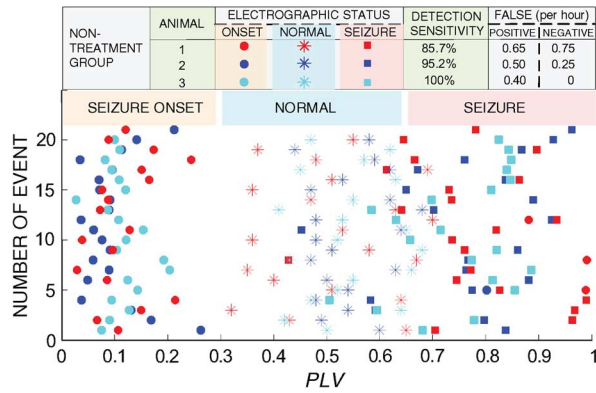


Fig. 10. Seizure onset detection performance for the non-treatment group.

C. Seizure Onset Detection Performance

The seizure onset detection performance was evaluated off-line, using intracranial EEG signals recorded from three animals in the non-treatment group. The basal EEG recordings and the induced epileptic seizure recordings were fed into the detector and the detection performance was characterized by calculating the detection sensitivity and the false positive and false negative rates. Fig. 10 demonstrates the seizure onset detection performance.

After PLV calculation, it was observed that basal/normal EEG signals had an average PLV in the range of 0.3 to 0.7, as shown in Fig. 11(a). However, the PLV dropped rapidly down to 0.2 at seizure onset and gradually increased to over 0.7 during the seizure, as shown in Fig. 11(b). Average detection sensitivity is 93.6 percent and average false positive and false negative frequencies are 0.52 and 0.33 times per hour, respectively. Fig. 11(c) shows an example of seizure onset detection and subsequent seizure suppression with self-triggered stimulation, explained in detail in the following sections.

D. Stimulator Experimental Characterization

The stimulator was experimentally characterized by loading it with an external resistor. Fig. 12 compares the measured and simulated input-output characteristic of the current driver.

Safety of current-mode stimulation is estimated using $Q = \sqrt{A} \times 10^k$, where Q is the charge per phase in μC , A is the electrode surface area in cm^2 , and k is a constant of 1.5 [19]. The electrode pad area is $110 \mu m \times 110 \mu m$ and the maximum deliverable charge per phase for the electrodes is $0.06 \mu C$ /phase in order to avoid tissue damage. Fig. 13 illustrates the current-mode stimulation safe region for different current amplitudes and pulse widths when using the presented nanotextured micro-electrode array (NME), and stimulation parameters chosen for each animal in the treatment group.

E. Seizure Suppression

The non-treatment group had 7 seizures per hour on average and their seizure behaviors were noted in Racine scale of 0 to 3 (0 = behavioral arrest (motionless), hair raising, excitement and rapid breathing; 1 = mouth movement of lips and tongue, vibrissae movements and salivation; 2 = head clonus and eye clonus; and 3 = forelimb clonus, wet dog shakes) [21]. An

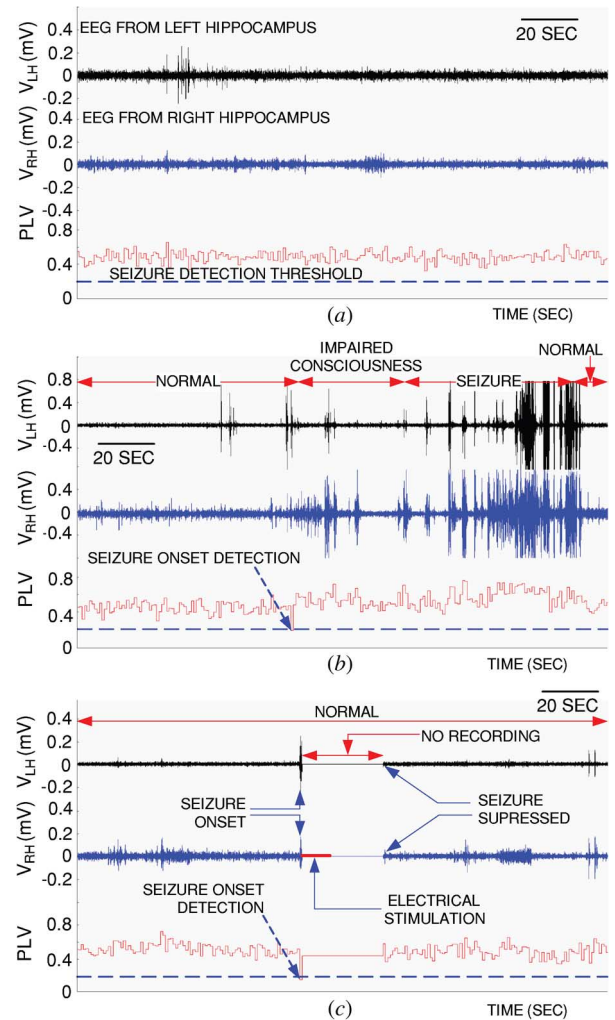


Fig. 11. Closed-loop stimulation triggered by seizure onset detection, V_{LH} is the EEG signal from the left hippocampus and V_{RH} is EEG signal from the right hippocampus, PLV is the synchrony index between V_{LH} and V_{RH} . (a) Basal EEG recordings and the corresponding PLV . (b) Induced electrographic seizure recordings and seizure onset detection using the PLV . (c) Automatic seizure onset detection, self-triggered electrical stimulation, and subsequent seizure suppression.

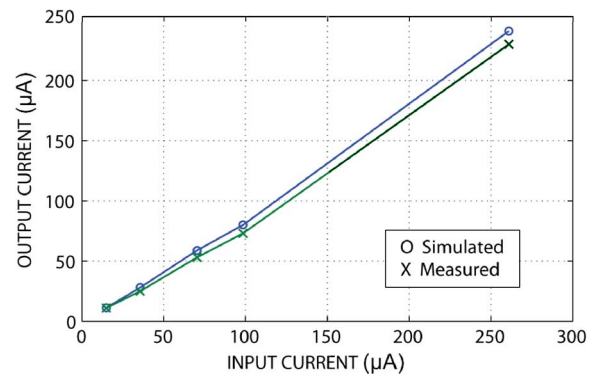


Fig. 12. Transfer characteristic of the current driver for $10 k\Omega$ load.

induced electrographic seizure is shown in Fig. 11(b) in which the PLV has dropped abruptly down to 0.2 at seizure onset.

The rats in the treatment group received electrical stimulation upon a seizure onset detection. The closed-loop stimulation system uses a low PLV value (seizure onset threshold = 0.2)

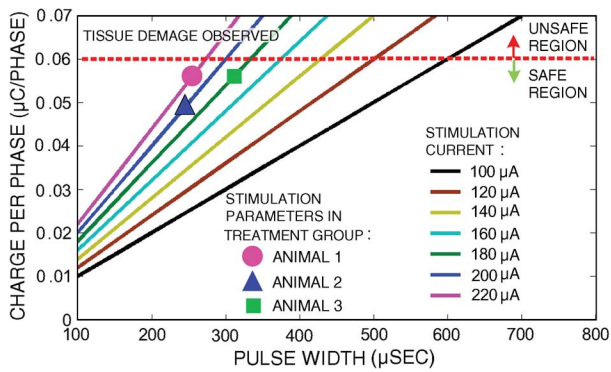


Fig. 13. Stimulation safe region for different current amplitudes and pulse widths when using the presented nanotextured microelectrode array (NME), and stimulation parameters chosen for each animal in the treatment group (3 rats).

TABLE I
EFFICACY OF THE SYSTEM IN SEIZURE SUPPRESSION

Parameter	Non-treatment (N=3)	Treatment (N=3)
4-AP dose	8 μ L	8 μ L
Seizure rate	7 per hour	0.17 per hour
False positive (false alarm)	0.52 per hour	0.4 per hour
False negative (missed)	0.33 per hour	0.17 per hour
Advance detection	35 sec	-
Detection sensitivity	93.6%	-
Seizure reduction	0%	92.8%

for triggering a 5 Hz 220 μ A monophasic stimulation current for 5 seconds in the hippocampus. Fig. 11(c) demonstrates the seizure onset detection, responsive electrical stimulation and seizure abortion. In this experiment, recording was temporarily disabled during stimulation in order to avoid stimulation artifact [26]. Late seizure detection (false negative) was observed 0.17 times per hour and false detections happened 0.4 times per hour. After the closed-loop stimulation, seizure frequency in treatment group dropped down to 0.17 times per hour on average (92.8 percent seizure rate reduction). The efficacy of the system in seizure onset detection and seizure rate reduction in the non-treatment group and treatment group rats is demonstrated in Table I.

F. Comparative Analysis

Table II compares the neuromonitoring and neurostimulation integrated circuit presented here to other reported designs. This system has the highest recording channels density at the cost of moderate power dissipation. The presented stimulator has a moderate number of channels and dissipates the least power.

A comparative analysis of the existing animal headsets is given in Table III. The presented headset prototype currently has 64 channels wirebonded for recording and 32 channels for stimulation. The number of channels can be scaled up to 1024 recording and 256 stimulation channels by full wirebonding on four stacked time-multiplexed neural amplifiers and stimulators modules. The other reported headsets have no or few stimulation channels. This work has the highest number of recording plus stimulation channels while dissipating least power.

TABLE II
COMPARATIVE ANALYSIS OF NEUROMONITORING AND NEUROSTIMULATION ICs

Reference	[27]	[28]	[29]	[30]	This work
Technology (μ m)	0.6	0.35	0.18	0.35	0.35
Area (mm^2)	42.25	10.9	2.7	0.72	12.77
Recording: No. of Ch.	128	2	8	16	256
Power/Ch. (μ W)	780	45	21.25	-	52
Stimulation: No. of Ch.	128	4	64	16	64
Power/Ch. (μ W)	150	-	7.4	-	2.6
Parallel operation	No	No	No	No	Yes

This prototype was designed for self-triggered closed-loop stimulation for treatment of epilepsy. Therefore, it includes ZigBee wireless transmission for a limited number of channels for optional remote neuromonitoring. The initial stage of the treatment includes recording EEG signals from all the channels with wired connection to delineate epileptogenic zone. In the next stage, stimulation is self-triggered upon seizure onset detection (Section II-C-5), while the wireless EEG recordings from a few channels can be monitored on a computer. Table III also shows that all the other headsets use commercial microelectrodes, but in this work custom-made smooth-surface and nanotextured microelectrode arrays were used in order to record good quality chronic EEG signals and stimulate on multiple channels. This design has a moderate size and weight and an adult rat (200 g) can readily carry the headset, which weighs approximately 6 percent of its body weight.

IV. CONCLUSION

A compact wireless rodent headset with a flexible microelectrode array have been demonstrated in neuromonitoring and neurostimulation in freely moving animals. The number of channels in the headset scales up to 1024 and 256, for neural recording and stimulation, respectively. Electrodeposition surface modification increases the effective surface area of the electrode contacts, yielding lower input impedance and improved interfacial capacitance. This translates into over 60 times reduction in the impedance at 100 Hz and four times less noise density compared to smooth-surface and commercial electrodes. Stimulation current is triggered once a seizure onset is detected in EEG recordings, using real-time digital signal processing in a remote computer or the on-board FPGA of the headset. The system features, including high-channel count in a small form factor, capability to both record and stimulate, flexible microelectrode arrays which enable high quality chronic recording and stimulation, and self-triggered closed-loop stimulation, shown to reduce seizure rate by 92.8 percent, differentiate this work and enable various novel responsive neurostimulation therapy experiments on freely moving animals.

TABLE III
COMPARATIVE ANALYSIS OF NEURAL STIMULATION AND RECORDING HEADSETS

Reference Year	HermesD [5] 2010	Neurochip-2 [4] 2011	Szuts et al. [31] 2011	Yin et al. [32] 2012	This work 2013
Recording:					
No. of channels	32	3	64	100	256
Input referred noise (μV)	2.4	2.7	4	8.5	8
Power/Ch. [mW]	2.1	101	2.6	6	0.013
Stimulation:					
No. of channels	N/A	N/A	3	N/A	64
Max power/Ch. (mW)	N/A	N/A	42	N/A	0.82
Die area [mm^2]	4.8×3.1	-	6.4×3	2×2	3.5×3.65
Wireless format	FSK	IR	RF	FSK	ZigBee
Electrodes	Utah (BlackRock Microsys., Inc.)	ECoG (Ad- Tech Medical Instrument Corp.)	Tetrode (Neuralynx Inc.)	Utah (BlackRock Microsys., Inc.)	Nanostructured- flexible
Total power (mW)	142	420	645	90.6	45
Size (mm^3)	$28 \times 28 \times 25$	$55 \times 35 \times 20$	$38 \times 38 \times 53$	$56 \times 42 \times 9$	$30 \times 22 \times 15$
Weight (g)	-	204	15	44.5	12

REFERENCES

- [1] M. Fifer, S. Acharya, H. Benz, M. Mollazadeh, N. Crone, and N. Thakor, "Toward electrocorticographic control of a dexterous upper limb prosthesis: Building brain-machine interfaces," *IEEE Pulse*, vol. 3, no. 1, pp. 38–42, Jan. 2012.
- [2] I. H. Stevenson and K. P. Kording, "How advances in neural recording affect data analysis," *Nature Neurosci.*, vol. 14, pp. 139–142, Jan. 2011.
- [3] Ripple: Grapevine Nano, Accessed Jun. 1, 2012 [Online]. Available: <https://www.rppl.com/products/grapevine-front-ends/item/133-grapevine-nano>
- [4] S. Zanos, A. G. Richardson, L. Shupe, F. P. Miles, and E. E. Fetz, "The neurochip-2: An autonomous head-fixed computer for recording and stimulating in freely behaving monkeys," *IEEE Trans. Neural Syst. Rehabil. Eng.*, vol. 19, no. 4, pp. 427–435, 2011.
- [5] H. Miranda, V. Gilja, C. Chestek, K. Shenoy, and T. Meng, "HermesD: A high-rate long-range wireless transmission system for simultaneous multichannel neural recording applications," *IEEE Trans. Biomed. Circuits Syst.*, vol. 4, no. 3, pp. 181–191, Jun. 2010.
- [6] R. Harrison, R. Kier, C. Chestek, V. Gilja, P. Nuyujukian, S. Ryu, B. Greger, F. Solzbacher, and K. Shenoy, "Wireless neural recording with single low-power integrated circuit," *IEEE Trans. Neural Syst. Rehabil. Eng.*, vol. 17, no. 4, pp. 322–329, Aug. 2009.
- [7] C. P. Young, S. F. Liang, D. W. Chang, Y. C. Liao, F. Z. Shaw, and C. H. Hsieh, "A portable wireless online closed-loop seizure controller in freely moving rats," *IEEE Trans. Instrum. Meas.*, vol. 60, no. 2, pp. 513–521, Feb. 2011.
- [8] J. Csicsvari, D. A. Henze, B. Jamieson, K. D. Harris, A. Sirota, P. Barthó, K. D. Wise, and G. Buzsáki, "Massively parallel recording of unit and local field potentials with silicon-based electrodes," *J. Neurophys.*, vol. 90, no. 2, pp. 1314–23, Aug. 2003.
- [9] R. Vetter, R. Miriani, B. Casey, K. Kong, J. Hetke, and D. Kipke, "Development of a microscale implantable neural interface (mini) probe system," in *Proc. 27th Annu. IEEE Int. Conf. Engineering in Medicine and Biology Soc.*, Jan. 2005, pp. 7341–7344.
- [10] R. H. Olsson and K. D. Wise, "A three-dimensional neural recording microsystem with implantable data compression circuitry," *IEEE J. Solid-State Circuits*, vol. 40, no. 12, pp. 2796–2804, Dec. 2005.
- [11] T. J. Reese, "Vagus nerve stimulation: A proven therapy for treatment of epilepsy strives to improve efficacy and expand applications," in *Proc. IEEE Engineering in Medicine and Biology Conf.*, 2009, pp. 4631–4634.
- [12] N. Sethi, D. Labar, L. Ponticello, J. Torgovnick, P. Sethi, and E. Arsur, "Treatment of medically refractory epilepsy: A review of vagus nerve stimulator," *Internet J. Neurol.*, vol. 9, no. 1, 2008.
- [13] M. B. Westover, J. Cormier, M. T. Bianchi, M. Shafi, R. Kilbride, A. J. Cole, and S. S. Cash, "Revising the 'Rule of Three' for inferring seizure freedom," *Epilepsia*, vol. 53, no. 2, pp. 368–376, Feb. 2012.
- [14] F. Rychlicki, N. Zamponi, R. Trignani, R. A. Ricciuti, M. Iacoangeli, and M. Scerrati, "Vagus nerve stimulation: Clinical experience in drug-resistant pediatric epileptic patients," *Seizure*, vol. 15, no. 7, pp. 483–490, 2006.
- [15] F. T. Sun, R. E. Wharen, and M. J. Morrell, "Responsive cortical stimulation for the treatment of epilepsy," *Neurotherapeut.*, vol. 5, no. 1, pp. 68–74, 2013.
- [16] T. L. Skarpaas and M. J. Morrell, "Intracranial stimulation therapy for epilepsy," *Neurotherapeut.*, vol. 6, no. 2, pp. 238–43, Apr. 2009.
- [17] R. S. Joseph, K. N. Fountas, A. M. Murro, D. Y. Park, P. D. Jenkins, M. Morrell, R. Esteller, and D. Greene, "Closed-loop stimulation in the control of focal epilepsy of insular origin," *Stereotact. Funct. Neurosurg.*, vol. 88, no. 5, pp. 281–287, 2009.
- [18] R. Shulyzki, K. Abdelhalim, A. Bagheri, C. Florez, P. Carlen, and R. Genov, "256-site active neural probe and 64-channel responsive cortical stimulator," in *Proc. IEEE Custom Integrated Circuits Conf.*, Sep. 2011.
- [19] R. V. Shannon, "A model of safe levels for electrical stimulation," *IEEE Trans. Biomed. Eng.*, vol. 39, no. 2, pp. 424–426, Feb. 1992.
- [20] S. Gabran, R. Mansour, and M. Salama, "Maskless pattern transfer using 355 nm laser," *Opt. Lasers Eng.*, vol. 50, no. 5, pp. 710–716, 2012.
- [21] R. J. Racine, "Modification of seizure activity by electrical stimulation: II. Motor seizure," *Electroencephalogr. Clin. Neurophys.*, vol. 32, pp. 281–294, 1972.
- [22] J. L. Perez Velazquez, L. G. Dominguez, V. Nenadovic, and R. A. Wennberg, "Experimental observation of increased fluctuations in an order parameter before epochs of extended brain synchronization," *J. Biol. Phys.*, vol. 37, pp. 141–152, 2011.
- [23] K. Abdelhalim, V. Smolyakov, and R. Genov, "A phase-synchronization epileptic seizure detector vlsi architecture," *IEEE Trans. Biomed. Circuits Syst.*, vol. 5, no. 5, pp. 430–438, 2011.
- [24] T. I. Netoff and S. J. Schiff, "Decreased neuronal synchronization during experimental seizures," *J. Neurosci.*, vol. 22, no. 16, pp. 7297–7307, Aug. 2002.
- [25] D. Gupta and C. J. James, "Narrowband vs. broadband phase synchronization analysis applied to independent components of ictal and interictal EEG," in *Proc. 29th Annu. Int. Conf. IEEE Engineering in Medicine and Biology Soc.*, Aug. 2007, pp. 3864–3867.
- [26] E. Brown, J. Ross, R. Blum, Y. Nam, B. Wheeler, and S. DeWeerth, "Stimulus-artifact elimination in a multi-electrode system," *IEEE Trans. Biomed. Circuits Syst.*, vol. 2, no. 1, pp. 10–21, Mar. 2008.
- [27] F. Heer, S. Hafizovic, W. Franks, A. Blau, C. Ziegler, and A. Hierlemann, "CMOS microelectrode array for bidirectional interaction with neuronal networks," *IEEE J. Solid-State Circuits*, vol. 41, no. 7, pp. 1620–1629, Jul. 2006.
- [28] M. Azin, D. J. Guggenmos, S. Barbay, R. J. Nudo, and P. Mohseni, "A battery-powered activity-dependent intracortical microstimulation IC for brain-machine-brain interface," *IEEE J. Solid-State Circuits*, vol. 46, no. 4, pp. 731–745, Apr. 2011.
- [29] J. Lee, H. Rhew, D. R. Kipke, and M. P. Flynn, "A 64 channel programmable closed-loop neurostimulator with 8 channel neural amplifier and logarithmic ADC," *IEEE J. Solid-State Circuits*, vol. 45, no. 9, pp. 1935–1945, Sep. 2010.
- [30] E. A. Brown, J. D. Ross, R. A. Blum, Y. Nam, B. C. Wheeler, and S. P. DeWeerth, "Stimulus-artifact elimination in a multi-electrode system," *IEEE Trans. Biomed. Circuits Syst.*, vol. 2, no. 1, pp. 10–21, Mar. 2008.

- [31] T. A. Szuts, V. Fadeyev, S. Kachiguine, A. Sher, M. V. Grivich, M. Agrochao, W. Hottowy, P. Dabrowski, E. V. Lubenov, A. G. Siapas, N. Uchida, A. M. Litke, and M. Meister, "A wireless multi-channel neural amplifier for freely moving animals," *Nature Neurosci.*, vol. 14, no. 2, pp. 263–269, 2011.
- [32] M. Yin, D. A. Borton, J. Aceros, W. R. Patterson, and A. V. Nurmikko, "A 100-channel hermetically sealed implantable device for wireless neurosensing applications," in *Proc. IEEE Int. Symp. Circuits and Systems*, May 2012, pp. 2629–2632.



Arezu Bagheri (S'11) received the B.A.Sc. degree in electrical and computer engineering from the University of Tehran, Tehran, Iran, in 2009.

Currently, she is working toward the M.A.Sc. degree in electrical and computer engineering at the University of Toronto, Toronto, ON, Canada. She was a Research Assistant at the Intelligent Sensory Microsystem Laboratory at the University of Toronto and her thesis focuses on DC-coupled digitally-assisted neural recording amplifiers. Her research interests include analog and mixed-signal

integrated circuit design for biomedical applications.

Ms. Bagheri was the recipient of the Ontario Graduate Scholarship in 2011.



S. R. I. Gabran (M'98) received the B.Sc. degree in electrical engineering from Cairo University, Cairo, Egypt, in 2002, and the M.A.Sc. and Ph.D. degrees in electrical engineering from the University of Waterloo, Waterloo, ON, Canada, in 2006 and 2012, respectively.

Currently, he is CTO and Director at Novela Inc. and a Researcher with the CIRFE Lab, University of Waterloo. His interests include micro-fabrication, neuro-engineering, intra-cortical implants, and BioMEMS.



Muhammad Tariqus Salam (M'09) received the B.A.Sc. degree in electrical and electronics engineering from the Islamic University of Technology, Gazipur, Bangladesh, the M.A.Sc. degree in electrical and computer engineering from Concordia University, Montréal, QC, Canada, and the Ph.D. degree in electrical engineering from Polytechnique Montréal, Montréal, QC, Canada, in 2003, 2007, and 2012, respectively.

Currently, he is a Postdoctoral Fellow at the University of Toronto, Toronto, QC, Canada, where he works in the Intelligent Sensory Microsystems Laboratory, Neurosciences and Mental Health Institute of Hospital for Sick Children Hospital, and the Neuroscience division of Toronto Western Hospital. His specific research interests are in the areas of biosensing, detection and stimulation microsystems, implantable biomedical microdevices for continuous health monitoring, cognitive brain research, mental disease diagnosis, treatment, and rehabilitations.



Jose Luis Perez Velazquez was born in Zaragoza, Spain. He received the "Licenciado" degree in chemistry (biochemistry, Universities of Zaragoza and Complutense of Madrid) and the Ph.D. degree from the Department of Molecular in Physiology and Biophysics at Baylor College of Medicine, Houston, TX, USA, in 1992, homologated to Doctorate in Chemistry by the Spanish Ministry of Culture in 1997.

Currently, he is an Associate Scientist in the Neuroscience and Mental Programme and the Brain and Behaviour Center at the Hospital For Sick Children, Toronto, ON, Canada, and Associate Professor at the University of Toronto, Toronto, ON, Canada.



Raafat R. Mansour (S'84–M'86–SM'90–F'01) was born in Cairo, Egypt, on March 31, 1955. He received the B.Sc. (with honors) and M.Sc. degrees in electrical engineering from Ain Shams University, Cairo, Egypt, in 1977 and 1981, respectively, and the Ph.D. degree in electrical engineering from the University of Waterloo, Waterloo, ON, Canada, in 1986.

In 1981, he was a Research Fellow with the Laboratoire de Electromagnetisme, Institut National Polytechnique, Grenoble, France. From 1983 to 1986, he was a Research and Teaching Assistant with the Department of Electrical Engineering, University of Waterloo. In 1986, he joined COM DEV Ltd., Cambridge, ON, Canada, where he held several technical and management positions with the Corporate Research and Development Department, becoming a Scientist in 1998. Since January 2000, he has been a Professor with the Electrical and Computer Engineering Department, University of Waterloo, where he was a Natural Sciences and Engineering Research Council of Canada (NSERC) Industrial Research Chair from 2001 to 2010. He currently holds a Canada Research Chair. He is the Founding Director of the Centre for Integrated RF Engineering. He has authored or coauthored numerous publications in the areas of filters and multiplexers, high-temperature superconductivity, and microelectromechanical systems (MEMS). He coauthored *Microwave Filters for Communication Systems* (Wiley, 2007). He holds several patents related to the areas of dielectric resonator filters, superconductivity and MEMS devices. His current research interests include MEMS technology and miniature tunable RF filters for wireless and satellite applications.

Dr. Mansour is a Fellow of the Engineering Institute of Canada (EIC) and the Canadian Academy of Engineering (CAE).



M. M. A. Salama (F'02) received the B.Sc. and M.Sc. degrees in electrical engineering from Cairo University, Cairo, Egypt, in 1971 and 1973, respectively, and the Ph.D. degree in electrical engineering from the University of Waterloo, Waterloo, ON, Canada, in 1977.

Currently, he is a Professor in the Department of Electrical and Computer Engineering, University of Waterloo. His interests include the operation and control of distribution systems, power-quality monitoring and mitigation, asset management, and electromagnetics. He has consulted widely with government agencies and the electrical industry.

Dr. Salama is a registered Professional Engineer in the Province of Ontario.



Roman Genov (S'96–M'02–SM'11) received the B.S. degree in electrical engineering from the Rochester Institute of Technology, NY, USA, in 1996, and the M.S.E. and Ph.D. degrees in electrical and computer engineering from The Johns Hopkins University, Baltimore, MD, USA, in 1998 and 2002, respectively.

He held engineering positions at Atmel Corporation, Columbia, MD, USA, in 1995 and Xerox Corporation, Rochester, NY, USA, in 1996. He was a Visiting Researcher in the Laboratory of Intelligent Systems at the Swiss Federal Institute of Technology (EPFL), Lausanne, Switzerland, in 1998 and in the Center for Biological and Computational Learning at Massachusetts Institute of Technology, Cambridge, MA, USA, in 1999. Currently, he is an Associate Professor in the Department of Electrical and Computer Engineering at the University of Toronto, Toronto, ON, Canada. His research interests are primarily in the area of implantable, wearable, and disposable biomedical electronics. This includes analog and digital VLSI circuits, systems and algorithms for electrical, chemical and photonic sensory information acquisition and energy-efficient signal processing with various medical applications such as brain-silicon interfaces and DNA microarrays.

Dr. Genov is a co-recipient of the Best Paper Award of the IEEE Biomedical Circuits and Systems Conference, Best Student Paper Award of the IEEE International Symposium on Circuits and Systems, Best Paper Award at the IEEE Circuits and Systems Society Sensory Systems Technical Committee, Brian L. Barge Award for Excellence in Microsystems Integration, MEMSCAP Microsystems Design Award, DALSA Corporation Award for Excellence in Microsystems Innovation, and Canadian Institutes of Health Research Next Generation Award. He was a Technical Program Co-Chair at the IEEE Biomedical Circuits and Systems Conference. He was an Associate Editor of IEEE TRANSACTIONS ON CIRCUITS AND SYSTEMS-II: EXPRESS BRIEFS and IEEE SIGNAL PROCESSING LETTERS. Currently, he is an Associate Editor of IEEE TRANSACTIONS ON BIOMEDICAL CIRCUITS AND SYSTEMS and serves on the Imagers, MEMS, Medical, and Displays Subcommittee of the International Solid-State Circuits Conference.